PERGAMON

International Journal of Heat and Mass Transfer 42 (1999) 2629–2647

International Journal of HEAT and MASS TRANSFER

Secondary flow and enhancement of heat transfer in horizontal parallel-plate and convergent channels heating from below

C. Gau[1]*, C.W. Liu[2], T.M. Huang[3], Win Aung[4]

Institute of Aeronautics and Astronautics, National Cheng Kung University, Tainan, Taiwan

Received 4 December 1997; in final form 5 August 1998

Abstract

Experimental studies of secondary air flow structure and enhancement of heat transfer in horizontal parallel-plate and convergent channels have been carried out. The bottom wall is horizontal and heated uniformly, while the opposite wall is insulated and inclined with respect to the horizontal plate so as to create a convergence angel of 3° for the convergent channel. The aspect ratio (width to height) and the ratio of channel length to height at the entrance of the channel is 6.67 and 15, respectively. The Reynolds number ranges from 100 to 2000, the buoyancy parameter, Gr/Re^2, from 2.5 to 907 and Pr of the air flow is 0.7. Flow structure inside the channel is visualized by injecting smoke at the inlet flowing along the bottom wall. The complete processes for the formation of the plumes associated with vortices and their transformation into longitudinal convection rolls due to the lateral extension and combination of the vortices are observed. The number of convection rolls formed is much less than those found in the experiments with water. For the convergent channel, the favorable pressure gradient causes a thinner bottom heated layer which results in much later initiation of secondary flow and fewer the number of plume produced. The interactions between neighboring vortices and plumes are suppressed by the acceleration of mainstream, and results in a stable flow and less pronounced enhancement of heat transfer. Temperature fluctuations at different locations are measured to indicate the flow structure and oscillation of the secondary flow. The effects of the buoyancy parameter and the convergence of the channel on the secondary flow structure and the Nusselt number are presented and discussed.

Nomenclature

b channel height at entrance
g gravitational acceleration
Gr Grashof number, $g\beta q(2b)^4/kv^2$
h convective heat transfer coefficient
$\bar{h}$ average heat transfer coefficient
k thermal conductivity of air
Nu local Nusselt number, $h(2b)/k$
$\overline{Nu}$ average Nusselt number, $\bar{h}(2b)/k$
Pr Prandtl number, v/α
q heat flux
Re Reynolds number defined at the inlet of the channel, $u_0(2b)/v$
T temperature
u_0 inlet velocity
x, y coordinate parallel, and normal to the heated wall.

Greek symbols
β coefficient of expansion
v kinematic viscosity.

Subscripts
b bulk mean
0 inlet.

* Corresponding author.
[1] Professor, Institute of Aeronautics and Astronautics.
[2] Graduate Student, Institute of Aeronautics and Astronautics.
[3] Graduate Student, Institute of Aeronautics and Astronautics.
[4] Adjunct Professor, College of Engineering, Southern Illinois University, Carbondale, IL, U.S.A. Permanent address: National Science Foundation, Arlington, VA, U.S.A.

0017–9310/99/$ - see front matter
PII: S0017–9310(98)00262–2

1. Introduction

Mixed convection in channels has received great interest in the last three decades for its practical application in solar energy collectors, heat exchangers, geothermal energy systems, chemical deposition of solid layer in the semiconductor industry, and cooling of nuclear reactors and modern electronic equipment. For horizontal channels heated from below, the buoyancy force can induce secondary flow which shortens the thermal developing length and enhance the heat transfer. The secondary flow is observed to be in the form of longitudinal vortex rolls which, as a result of the shear force imposed by the mainstream, begin to bifurcate and curl back to the heated surface such that a mushroom configuration is seen when viewed in the spanwise direction. It is found that the flow structure and heat transfer depends on the Rayleigh number, the Reynolds number, the Prandtl number and the aspect ratio (width to height ratio) of the channel. For the parallel-plate channel experiments with water, a complete flow process for the formation of plumes and the resulting mushroom-shaped vortices and their effect on the heat transfer have been well studied [1, 2]. For the experiments with air, the formation of plumes in the upstream region [3, 4] and the longitudinal convection rolls in the fully developed region [5] have also been studied. The complete transformation process from a plume flow into the longitudinal convection rolls has not been studied. Due to the difference in the Pr number, the complete transformation process for the experiments with water may not be used to infer the experiments with air. For the convergent channel, the convergence of channel can accelerate the mainstream which results in suppressing the turbulence and reducing the buoyancy effect. It may completely change the transformation process and greatly alter the secondary flow structure and the heat transfer. In order to understand these processes and effects, a systematic study on the mixed convection flow and heat transfer of air in both the parallel-plate and the convergent channel is performed.

The earlier work on the mixed convection, especially the secondary flow structure and its effect on the heat transfer, in the parallel-plate channel was made by Mori and Uchida [5] who apply the linear stability theory to analyze the fully developed buoyancy induced secondary flow in an asymmetric isothermal channel. Both the first and second type vortex rolls are predicted. Longitudinal convection rolls are observed in the experiments with air which are used to check the validity of the analysis. In the developing region, Hwang and Liu [3] observe the mushroom-shaped plume associated with vortices and found that the wave length of the plume decreases and approaches the prediction based on the linear stability analysis as the aspect ratio increases. For the experiments with water, the complete transformation process of the secondary flow from the mushroom-shaped plume to the vortices, the breakdown of vortices and the transition to the turbulent flow is visualized [6, 7]. For $Gr \leqslant 1.5 \times 10^7$, the number of plume produced is $A/2$, but with increasing Gr to 8.0×10^8, the number increases to approximately $4A$. This behavior is consistent with the results for the experiments with water [1, 8]. However, in the experiments with air [4, 9], the periodic spanwise temperature distributions with wavelength of the channel height have been measured and obtained when $Ra \geqslant 8000$, which suggests the appearance of the second type vortex rolls as predicted by Mori and Uchida. The critical Rayleigh numbers for the onset of secondary flow were also studied in the fully developed region [10–12] and both the thermal entry and the combined entry region [2, 4, 13, 14]. Correlations for the onset of thermal instability are obtained for both the experiments with water and air. It is found that as the critical Rayleigh number increases, the onset of instability moves upstream and the corresponding wave numbers increase. Theoretical analyses [15–17] were also performed to predict the onset of the thermal instability. The predictions are close to the experimental data. For the heat transfer, significant enhancement in the heat transfer due to the secondary flow is found. However, longitudinal periodicity in the Nusselt number upstream of the fully developed region are found only in the experiments with water [6, 7], but are not reported in the experiments with air [2, 14]. From the review of literature, it appears the results obtained for the critical Rayleigh number for the initiation of the plume, the number of plume produced and the heat transfer characteristic between the experiments with water and the ones with air are different.

Numerical studies are also performed to study the occurrence and the structure of the secondary flow and the enhancement of heat transfer in both the developing and fully developed regions [18–23]. The trends obtained in general are consistent with the experimental observations. However, most of the numerical calculations assume steady laminar flow. This may not be true for the initiation and growth of the plumes and vortices. Further improvement in the numerical calculation is still needed.

An extensive review of the published reports on mixed convection in a horizontal channel has turned up no study on the effect of buoyancy in the horizontal convergent channel. The prior studies on the flow and heat transfer in a convergent or a divergent channel are mostly concerned with pure forced convection. By assuming that the family of straight lines passing through the source or sink constitute the streamlines of the flow, the governing equations of the system can be greatly simplified. This type of flow is called Jeffery–Hamel flow. The thermal flow of Jeffery–Hamel flow with constant wall temperature or a variation in wall heat flux according to $q_w \sim 1/r$, where r denotes the axial distance from the source or the sink of the flow, has been studied [24, 26]. For developing flow, it has been found that the Nusselt number increases with

the convergence angle [27, 28]. Su and Lin [29, 30] obtain the numerical results for both convergent and divergent ducts and conclude that both the pressure drop and the Nusselt number increase with the convergent or the divergent angle. Experiments were also performed in a convergent channel [31, 32] and the results indicate that the acceleration of flow due to convergence of channel can suppress the turbulence and promote re-transition to a laminar flow. To consider the buoyancy effect, Gau et al. [33], appears to be the first experimental work to study mixed convection in a divergent channel. It appears that mixed convection flow and heat transfer data in a channel with one wall inclined at a small angle are still very lacking. These kinds of geometric configurations have practical applications in electronic coolings [34, 35].

The present paper describes an experimental study of mixed convection in a heated horizontal parallel-plate or convergent channel. A uniform air flow is provided at the entrance, and exits to the ambient after passing through the channel. The bottom wall is maintained in the horizontal position and is heated uniformly. For the convergent channel, the opposite, top wall has a convergence angle of 3° to the horizontal plane. That is, the downstream end of the top wall is tilted toward the bottom wall, and is well insulated. The objective of this investigation is to study the mixed convection flow, especially the secondary flow structure and the heat transfer, in a heated horizontal parallel-plate or convergent channel. Results of both the flow visualization by introducing smoke at the inlet and the heat transfer measurements along the heated wall are presented. The effects of the buoyancy parameter and the Reynolds number on the flow structure and the Nusselt number are reported.

2. Experimental apparatus and procedures

Experiments are performed in a Plexiglass channel. The channel is 45 cm in length, 20 cm in width inside and 3 cm in height at the entrance. The heated wall is kept horizontal and the opposite wall is tilted with a convergence angle of 3°. The heated wall is made of 2 cm thick balsa wood and electrically heated. This is achieved by gluing a number of 0.015 cm thick stainless steel foil strips on the entire bottom wall and passing an electric current through the foil heater. DC power is used to provide the electric energy for generating the desired heat flux. The heat flux can be determined by the electric voltage and current passing through the foil. The electric voltage drop due to the contact resistance between the heating strips and the terminals, which connect the heating strips with the DC power supply, has been taken into account. This kind of voltage drop is also noticed in other experiment [36]. For better insulation, a 12 cm thick foam rubber is glued on the back of the heated wall. All the other side walls are wrapped with 3 cm thick foam rubber.

Since the temperature variation of the heated wall may be large in the transverse direction, the heated wall is instrumented with seven rows of chromel-alumel thermocouples. One row of the thermocouples is along the centerline of the wall. The distance between two neighboring rows is 2.5 cm, and the spacing between two neighboring thermocouples in each row is 1 cm. Since the surface temperature of the insulated wall is needed for estimating the radiation loss from the heated wall, five additional thermocouples are embedded along the surface of the wall. All thermocouples are calibrated in a constant temperature bath and the measurement error is found to be within ± 0.1°C. All the temperature signals are acquired with a FLUKE-2287A data logger connected to a computer for direct processing. The temperature data are taken when the entire system reaches steady state, usually in 3–4 h.

During the flow visualization experiments, a smoke generator is used to supply smoke of fine particles. The smoke particles are measured to be in a scale of 2 μm and are small enough to trace the flow in the channel. Smoke enters the channel from a slot of 1 mm width located on the bottom surface in the immediate upstream of the channel entrance. A transverse sheet of light perpendicular to the top insulated wall is used to visualize the spanwise structure of secondary flow; while the sheet of light from the end parallel to the flow passage is used to visualize the flow structure from the top view. The flow patterns at the upstream, the central and the downstream regions can be observed and recorded. The smoke particles injected were found to have no obvious effect on the heat transfer after rerunning the heat transfer measurements. During the experiments, the flow structure in the channel is sensitive to the circulation of ambient flow. Therefore, a wind shield is constructed around the exit of the channel to prevent this possible extraneous effect.

The wind tunnel is the same as the one used in the studies of mixed convection in a heated vertical convergent or divergent channel [33–35]; hence, a detailed description is omitted here. The calibration needed for velocity measurement is also described in these reports. The total heat input in a single heating strip can be determined by the electric voltage and current passing through the strip. Since both conduction and radiation losses from each heating strip need to be accounted for and subtracted from the total energy supplied by the heater, the local heat transfer coefficient is evaluated by the following equation:

$$h_r = (q_t - q_{rad} - q_{\mathrm{cond}})/(\bar{T}_w - T_r) \tag{1}$$

where $\bar{T}_w$ is the average temperature of a single strip, and r refers to the bulk mean condition or the inlet condition. The conduction loss from the heated wall is estimated by a one-dimensional conduction equation in a composite

wall. The procedure to calculate the radiation loss from the heated wall is very similar to the one described in [36] and will not be repeated here. The thermophysical properties used in the local Nusselt number are evaluated at the bulk mean temperature of the flow, while those in the Reynolds and Grashof numbers are evaluated at the inlet temperature.

Since the channel flow exits directly to the ambient, the heat loss is relatively large near the exit. Therefore, the last three heating strips are used only as guard heaters. Relatively large heat loss in the exit region is also found in other experiments [36, 37]. The uncertainty of the experimental data is determined according to the procedure proposed by Kline and McClintock [38]. The maximum uncertainty of local Nusselt number is 5.6%, while that for the Reynolds and Grashof number are 6.2 and 7.8%, respectively.

3. Results and discussions

3.1. Flow visualizations

3.1.1. Parallel-plate horizontal channel

The smoke exits from a spanwise, narrow slot on the bottom wall of the channel at the inlet, and enters smoothly into the channel forming a thin sheet of smoke along the bottom wall. As the thin-sheet smoke is heated, it becomes unstable and protrudes upward like a plume. The protrusion of plume make the bottom heated layer thinner and cause a higher rate of heat transfer. Figure 1a shows the top view close to the mid-height while Fig. 1b–e shows the end view of the secondary flow at different streamwise locations. The convergence of the smoke streaks in Fig. 1a suggests the formation of the rising plumes from the bottom wall where the mushroom-shaped plume has not yet developed. The divergence of smoke streaks in the downstream suggests the formation of mushroom head as shown in Fig. 1c and d, which extends spanwisely and forms a pair of circulation vortices. The earliest formation of plume occurs in the corners near the side walls where the flow velocity is relatively low and the bottom heated layer is relatively thick which readily causes protrusion of plume, while the latest formation of plume occurs near the center region where the flow velocity is much higher and the bottom heated layer is relatively thin, as shown in Fig. 1c where the plume in the central region have just occurred and they appears as small buds. Similar phenomenon was also observed in the experiments for water [7]. Excluding the plumes by the side walls, the number of plumes produced is four for $Gr/Re^2 = 20$ ($Gr = 5 \times 10^6$) and $Re = 500$. As the flow moves downstream, the bottom heated layer becomes thicker and the temperature becomes higher due to the heat input along the bottom wall. This leads to the growth of plumes, i.e., the rise of plume height and lateral extension of the mushroom head. This causes the lateral extension of circulation vortices and results in the interaction between the neighboring vortices, as shown in Fig. 1d and e, especially the two vortices on the corners which are the earliest to interact with the neighboring vortices and form a complex flow structure.

The lateral extension of the circulation vortices was not found in the experiments with water [1, 7]. Instead, the circulation vortices parallel to each other and form longitudinal vortices. The mechanism for the lateral extension of the circulation vortices in the experiments with air may be attributed to the lower Pr and higher α values that the thermal diffusion and convection from circulation vortex to the surroundings is more rapid than in the water. A comparison of the plumes and vortices formed in the experiments with water [7], one can find that the number of the plumes produced in the current experiments is much less and the size of the plumes is much greater. This difference is attributed again to the difference in the Pr number of the fluid. For large Pr, the bottom heated layer (thermal boundary layer) becomes thinner and resulting the protrusion of the thermals thinner and smaller. Therefore, to compare the number of plumes produced between the experiments with water and the ones with air, the Pr number should be taken into account. Therefore, instead of using Gr, the dimensionless parameter $Gr \times Pr = Ra$ is suggested to use. It is found that at the same Rayleigh number the number of plumes produced in the current experiments is approximately equal to the ones in the experiments with water.

As the buoyancy parameter increases, the bottom heated layer becomes thicker. The initiation of plumes and formation of mushroom head occur at a much earlier stage and the number of plumes initiated increases. These findings agree with the one reported in [7]. For $Gr/Re^2 = 60$, $Re = 500$, by excluding the two plumes in the corners, there are a total of five plumes and the spacing between each plume is close to the height of the channel [35]. In the downstream, the growth of plume and lateral extension of the mushroom head leads to a strong interaction of vortices. Not only that the interaction can occur at an earlier stage but also the interaction is highly unstable and form a very complicated flow structure, as shown in Fig. 2 d and e. Some of the plumes may shrink and disappear. Some of the vortices may oscillate in the spanwise direction. However, no breakdown of vortices and transition to the turbulent flow is found as described in the experiments with water. This is also true within the range covered by the current experiments. Some of the vortices may combine with others which leads to the development of longitudinal convection rolls, as shown in Fig. 2 g.

For the case of the $Re = 105$ and $Gr/Re^2 = 450$ ($Gr = 4.96 \times 10^6$), the mainstream velocity is relatively low and the buoyancy parameter is large. However, excluding the plumes produced by the side walls, the number of

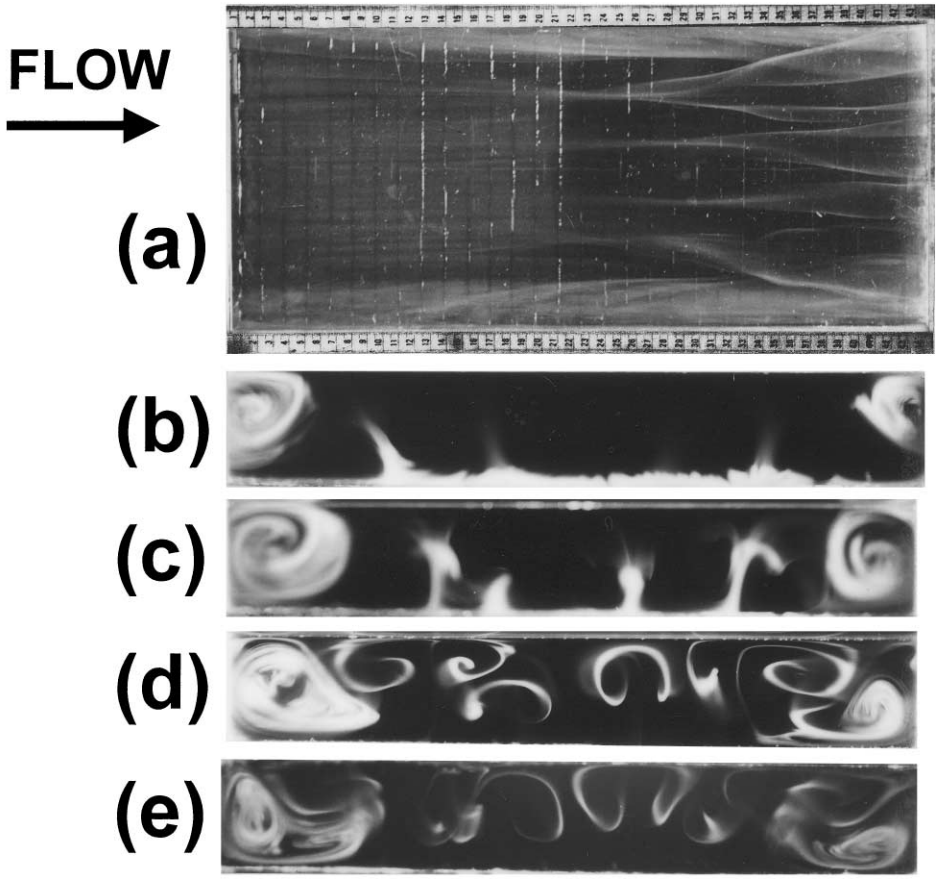

Fig. 1. Flow structure in a horizontal parallel-plate channel with $Gr/Re^2 = 20$ and $Re = 500$; (a) top view; (b) end view at $x = 15$ cm; (c) $x = 25$ cm; (d) $x = 36$ cm; (e) $x = 43$ cm.

plumes produced is four (Fig. 3b) which is equal to the case of $Re = 500$ and $Gr/Re^2 = 20$ ($Gr = 5 \times 10^6$). It appears that the number of plumes produced is not proportional to the buoyancy parameter, but proportional to the Grashof or the Rayleigh number. This trend agrees with those reported in [1, 8]. The well established longitudinal convection rolls can be formed near the exit of channel, as shown in Fig. 3. Although the top view of flow structure in the downstream location, as shown in Fig. 3a, does not indicate a regular flow structure of laminar convection, the end view clearly indicates that the flow is not turbulent. Similar conclusion concerning the existence of laminar flow structure can also be made from the temperature fluctuation measurements. Since the combination process between the two neighboring vortices was not found in the experiments with water, the number of the longitudinal convection rolls found in the experiments with water should be twice the number of the convection rolls formed in the experiments with air. During the formation of the convection roll, the corner vortex can also combine with its neighboring vortex and form longitudinal convection roll. By counting the two plumes produced by the side walls as one, the number of plumes initiated in the upstream region for $Re = 105$ and $Gr/Re^2 = 450$ is five. Therefore, the number of convection rolls formed is expected to be five. However, the convection rolls formed in the downstream is four, as shown in Fig. 3c. This difference is due to the fact that during the combination process some of the plumes may completely disappear, the number of convection roll is less than what one can expect.

For $Re = 1000$ and $Gr/Re^2 = 10$ ($Gr = 10^7$), in comparison with the case of $Re = 500$ and $Gr/Re^2 = 10$ [35] the Reynolds number is double, and the Grashof number increases quadruply. Therefore, the initiation of plume occurs at a much earlier stage, and the number of plumes initiated, as expected, are greater than the case of $Re = 500$ and $Gr/Re^2 = 10$ ($Gr = 2.5 \times 10^6$). For the former case, the number of plumes produced is five; while in the latter case (Fig. 4), the number of plumes produced is four [35]. Therefore, one can conclude that the number of plumes produced is neither affected by the buoyancy parameter, nor affected by the Reynolds number. However, the type of flow structure (mushroom-shaped

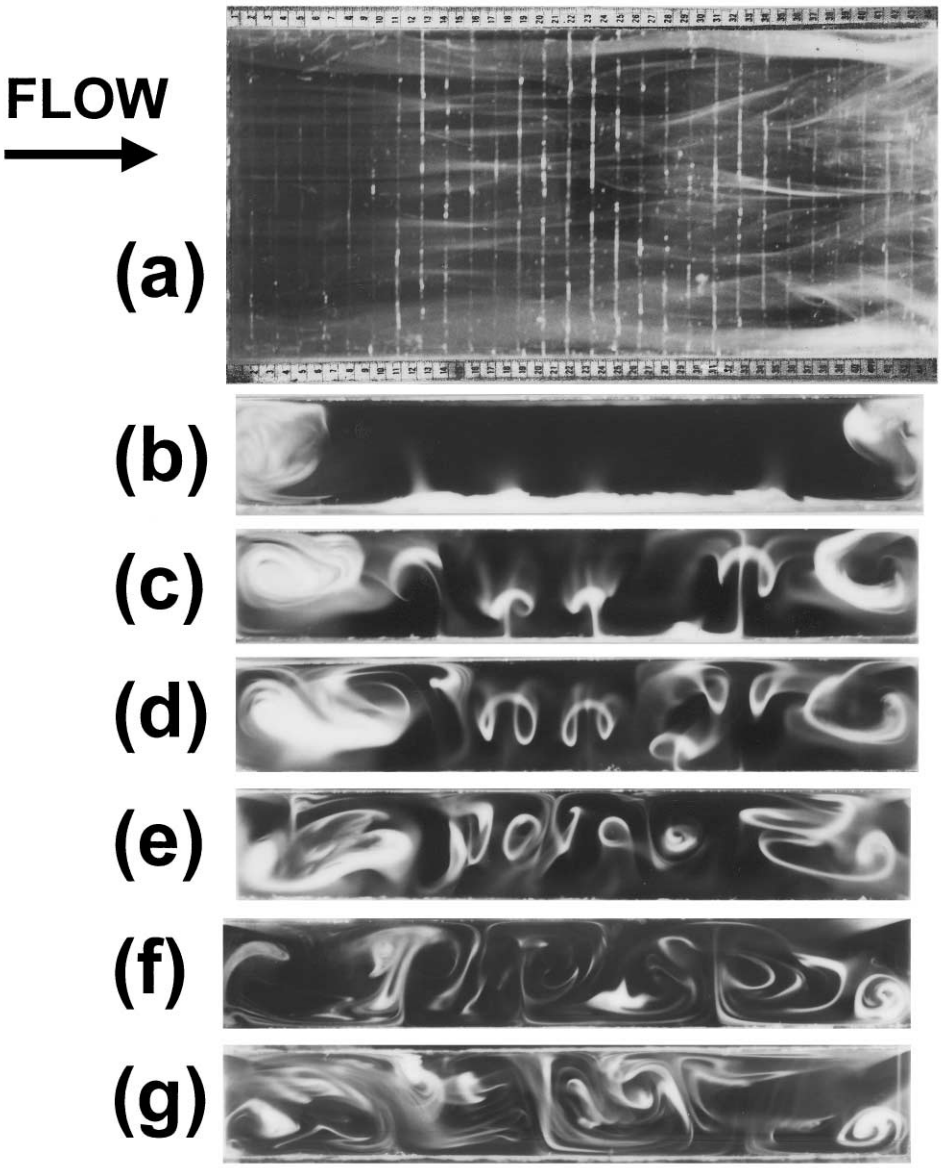

Fig. 2. Flow structure in a horizontal parallel-plate channel with $Gr/Re^2 = 60$ and $Re = 500$; (a) top view; (b) end view at $x = 8$ cm; (c) $x = 15$ cm; (d) $x = 20$ cm; (e) $x = 25$ cm; (f) $x = 36$ cm; (g) $x = 43$ cm.

plume or convection roll) is indeed significantly affected by these two parameters. Therefore, the parameters selected for presentation of the flow structure varies differently in different reports. It depends on what one would like to see. Since the streamwise velocity is relatively high as compared with the lateral extension of vortices, interaction between vortices is not found. However, at this high Re and Gr, the plume and vortex formed is not stable. This is attributed to the relatively high speed of mainstream flowing over a relatively thick heated layer in the bottom wall. It is found that at higher value of Re with the same value of Gr/Re^2, the plume and the vortex produced become more unstable. New plume may be initiated as shown in Fig. 4d and e, which sucks away the bottom heated layer and cause the neighboring plumes to shrink. Some of the plume may expand or shrink, as shown in Fig. 4e and f, or they may oscillate in spanwise direction and interact occasionally with the neighboring plume, as shown in Fig. 4g. Although the vortex flow is highly unstable, no transition to the turbulent flow as those occurred in the experiments with water [7] is found.

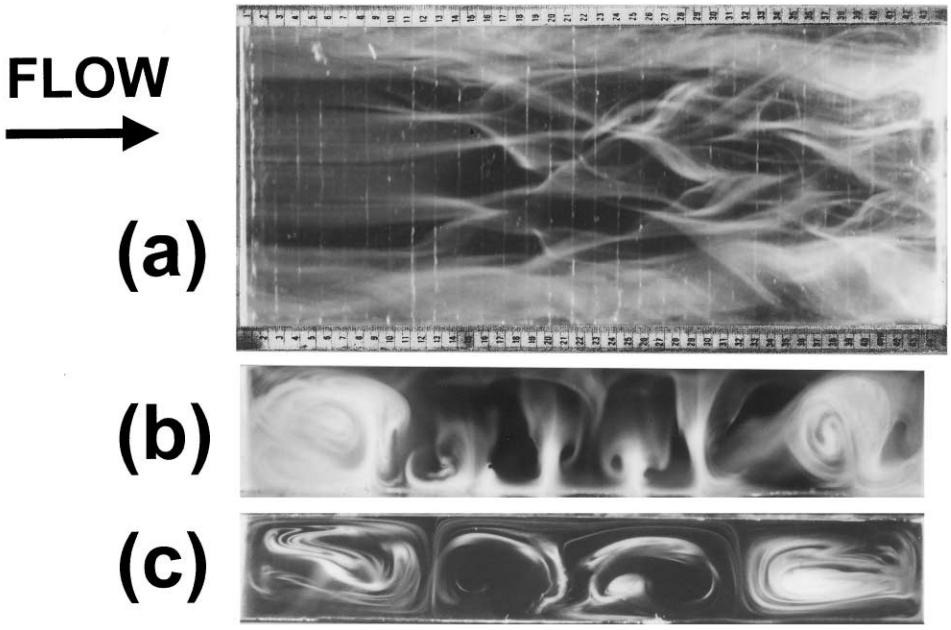

Fig. 3. Flow structure in a horizontal parallel-plate channel with $Gr/Re^2 = 450$ and $Re = 105$; (a) top view; (b) end view at $x = 15$ cm; (c) $x = 43$ cm.

3.1.2. Convergent channel

The convergence of channel accelerates the flow. At the same time the favorable pressure gradient tends to stabilize the flow. For $Gr/Re^2 = 10$ and $Re = 500$, the sheet of heated smoke moves steadily downstream. No initiation of plume and vortex is found, as shown the end view in Fig. 5a, as those plumes formed in the parallel-plate channel. This is attributed to the acceleration of flow which makes the heated bottom layer thinner and protrusion of the heated layer impossible. Without initiation of plume, the buoyancy force is not expected to play an important role to affect and enhance the heat transfer. Fig. 5a–d are the end view at the exit of the channel. The height of the channel at the exit is 0.64 cm. For $Gr/Re^2 = 20$ and $Re = 500$, plumes are produced close to the exit, as shown in Fig. 5b. Excluding the two plumes produced in the corners, there are a total of four plumes. The space between the neighboring plumes is greater than the channel height. Two plumes produced in the central region appear as a small bud where the two plumes closer to the side walls appear as mushroom shape. It appears that the initiation of the plumes has been delayed at a later stage due to the stabilization effect of the acceleration. For $Gr/Re^2 = 40$ and $Re = 500$, initiation of plumes occurs close to the middle of the channel, which is approximately at $x = 22$ cm, as shown in Fig. 5e, where the thermal streak has converged to an extreme point and started to diverge thereafter. It appears that mushroom-shaped vortex extend slowly in the lateral direction until close to the neighboring vortex. However, the lateral extension of vortex stops as it approaches the neighboring one and does not interact with the neighboring vortex. It appears that acceleration of flow can stabilize the flow and suppress the unstable interaction between vortices. For $Gr/Re^2 = 60$ and $Re = 500$, interaction between vortices is still not found as shown in Fig. 5d and f, due to the stabilization effect of the accelerating flow. By excluding the two plumes produced in the corners, there are still a total of four plumes. The number of plume produced in this case is less than the case for the parallel-plate channel and the divergent channel. This is apparently attributed to the acceleration of flow which can make the heated bottom layer thinner and protrusion of the heated layer become difficult. The flow observed is highly stable for the experimental ranges covered.

3.2. Temperature fluctuations

3.2.1. Parallel-plate channel

A very thin thermocouple probe having wire diameter of 0.1 mm is placed 5 mm above the heated wall to measure the temperature fluctuations along the centerline at different streamwise locations. For $Gr/Re^2 = 20$ and $Re = 500$, no fluctuations of temperature is found, as shown in Fig. 6a when the bottom heated layer is still very thin and stable, and plumes in the central region is not initiated. Small temperature fluctuations is initiated, as shown in Fig. 6b for $x = 25$ cm, when the bottom heated layer becomes very thick and unstable, initiation of small bud and formation of mushroom-shaped plume

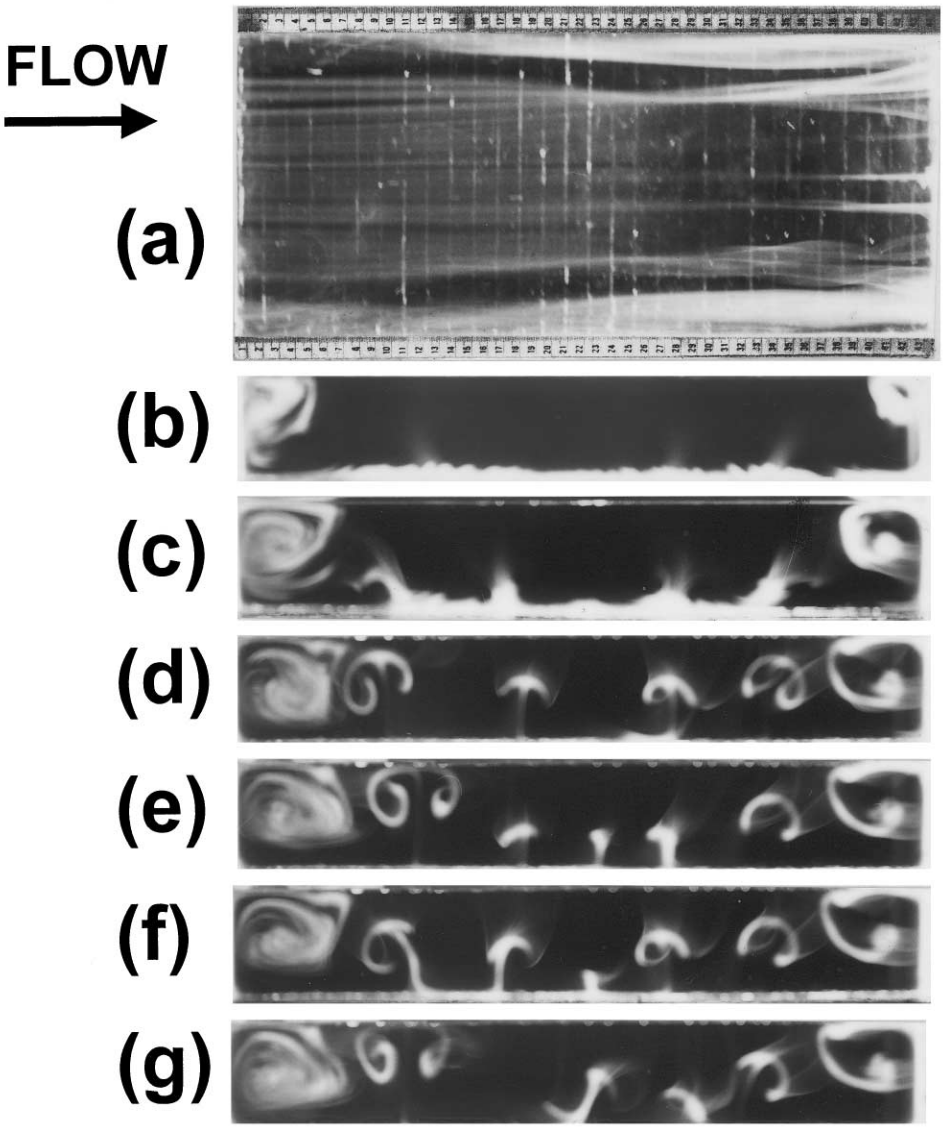

Fig. 4. Flow structure in a horizontal parallel-plate channel with $Gr/Re^2 = 10$ and $Re = 1000$; (a) top view; (b) end view at $x = 15$ cm; (c) $x = 25$ cm; (d)–(g) $x = 36$ cm.

associated with vortices occur. The amplitude and frequency of temperature fluctuation increases as flow moves downstream, as shown in Fig. 6c and d. This is attributed to the oscillation and interaction of plumes and vortices as shown in Fig. 1d and e. However, the relatively small amplitude of temperature fluctuation suggests that the interaction between vortices is not so intense to cause a highly unstable flow and even transition to turbulent flow. Another contribution to the intense fluctuations of temperature in the downstream region is due to that the oscillation of flow generated upstream can propagate downstream. It appears that the oscillation of flow generated downstream will not propagate upstream.

As the thermocouple moves downstream, the mean temperature rises gradually as shown in Fig. 6 for $Gr/Re^2 = 20$ and $Re = 500$, due to the heat input along the bottom wall which makes the bottom heated layer thicker and its temperature higher. However, a gradual decrease in the mean temperature occurs after $x = 25$ cm as shown in Fig. 6b, c and d. Flow visualization indicates that both plume and vortex activities are very intense in this region. Therefore, the decrease in mean temperature is attributed to the intense activity of plume and vortex which suck

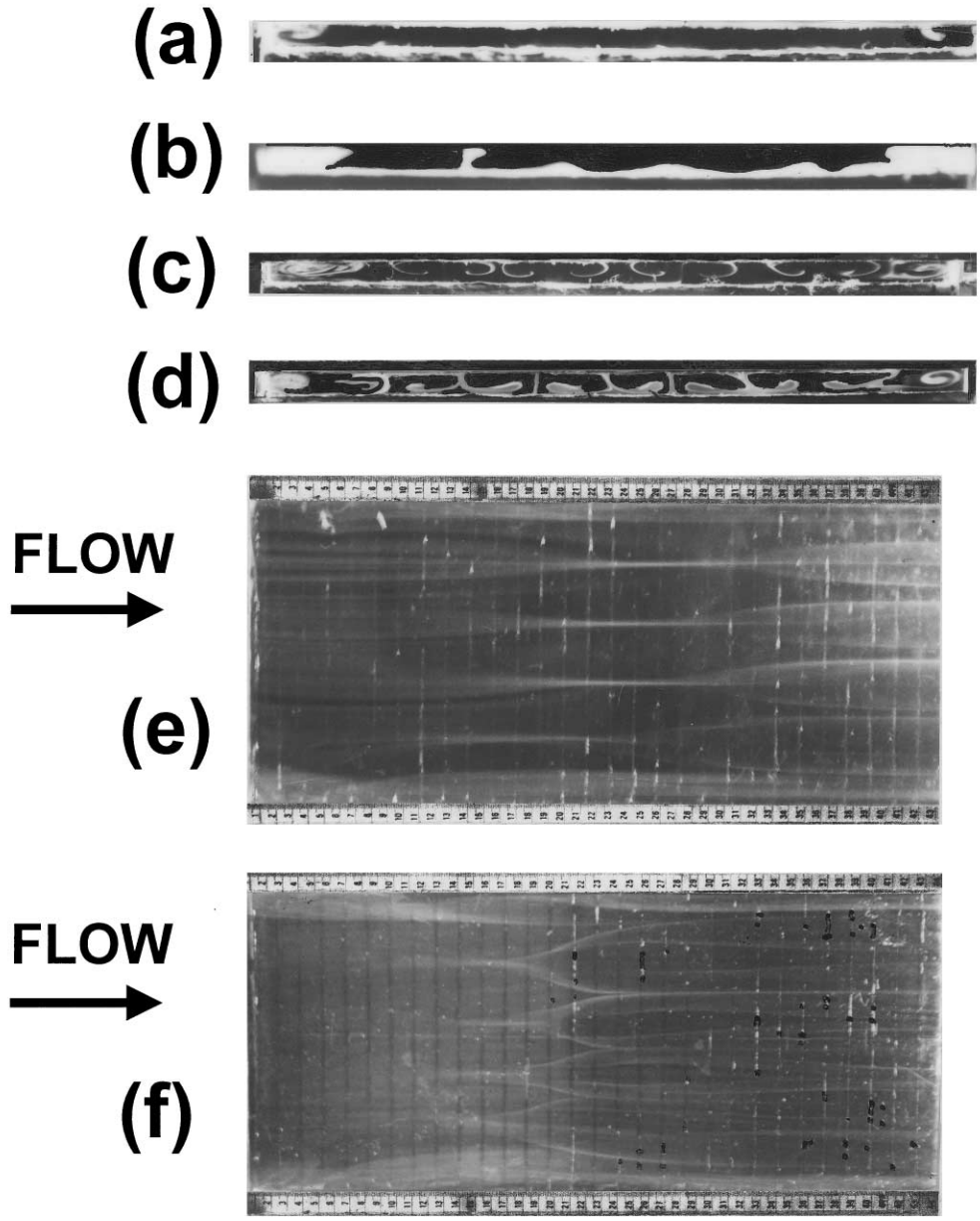

Fig. 5. Flow structure in a horizontal convergent channel with $Re=500$ and (a) $Gr/Re^2=10$; (b) $Gr/Re^2=20$; (c) $Gr/Re^2=40$; (d) $Gr/Re^2=60$ for end view; (e) $Gr/Re^2=40$; (f) $Gr/Re^2=60$ for top view.

away some of the fluid in the bottom heated layer and makes this layer thinner. The continuous and gradual decrease in the mean temperature toward downstream suggests that the plume and vortex activities is getting intense as flow moves downstream. Due to the thin bottom layer, the heat transfer in this region is expected to be enhanced.

For $Gr/Re^2=60$ and $Re=500$ where buoyancy parameter is relatively large, initiation of mushroom-shaped plume associated with vortices can occur at a much earlier stage, which is close to $x=15$ cm as shown in Fig. 2c, and cause fluctuation of temperature, as shown in Fig. 7b. At this high buoyancy parameter, the number of plumes initiated increases. There is one plume occurring close to the centerline which causes fluctuations of significantly large amplitude, as shown in Fig. 7c and d. However, when the plume moves away from the center line, the amplitude of fluctuation reduces significantly. This

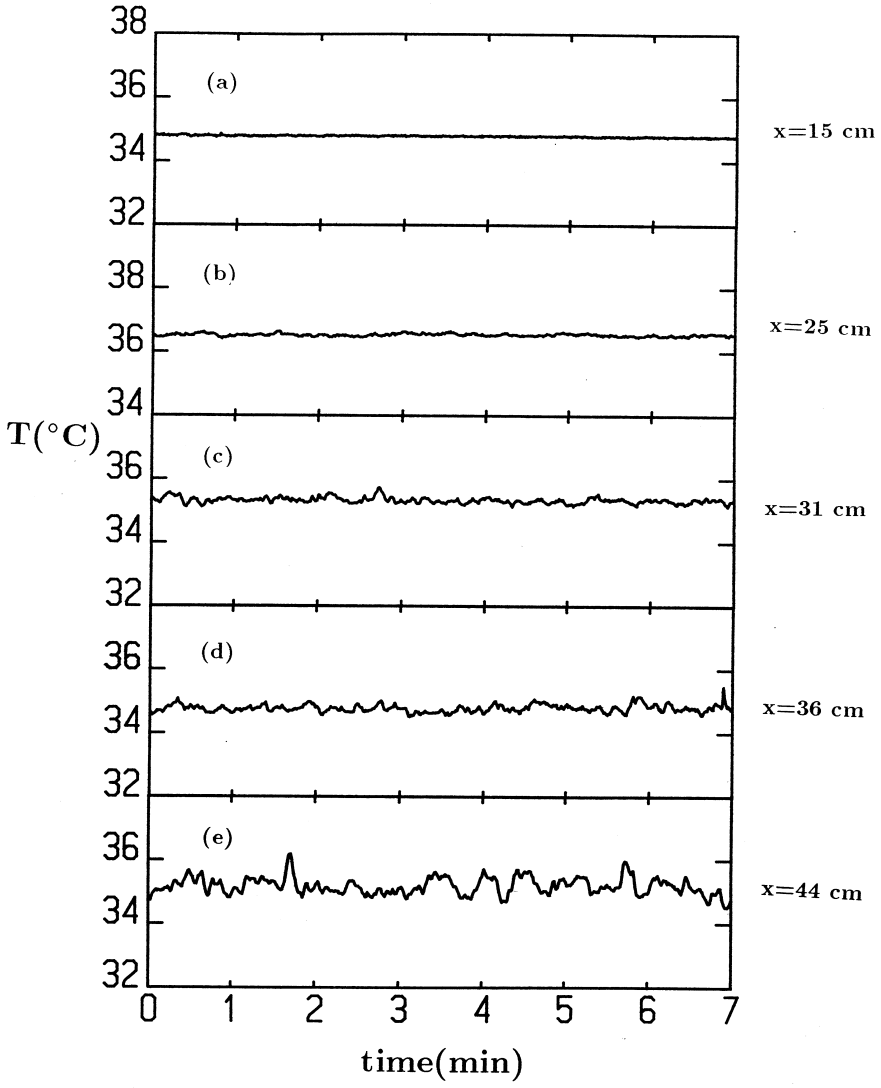

Fig. 6. Temperature fluctuations in a horizontal parallel-plate channel with $Gr/Re^2=20$ and $Re=500$ at (a) $x=15$ cm; (b) $x=25$ cm; (c) $x=31$ cm; (d) $x=36$ cm; (e) $x=44$ cm.

suggests the spanwise oscillation of the plume, which agrees with the results of the previous flow visualization. Even the complex flow structure due to interaction between vortices does not cause a significant variation of temperature. The small amplitude of temperature fluctuations suggests that the complex flow is not turbulent. It can be expected that the complex flow structure occurred will not significantly enhance the heat transfer. Since the rising plume can reduce the thickness of the bottom heated layer, this action is the major mechanism to cause enhancement of heat transfer. The relatively large amplitude of temperature fluctuation near the exit, as shown in Fig. 7f, is attributed again to the fact that the thermocouple probe is actually located in the region where plume passes through, and is not occurrence of turbulence. Excluding the time period when plume passes through the probe and causes significant increase in temperature, a decrease in mean temperature also occur from $x=15$ cm to $x=25$ cm, as shown in Fig. 7b and c. This suggests that a significant enhancement in heat transfer by the secondary flow from $x=15$ cm to $x=25$ cm can be expected. For $x>25$ cm, however, the mean temperature increase gradually, no significant enhancement in heat transfer is expected. The heat transfer measurements in the next section has confirmed this result.

For $Gr/Re^2=340$ and $Re=105$, the mainstream velocity is relatively low while the buoyancy force is large. The temperature fluctuation starts to occur at an earlier

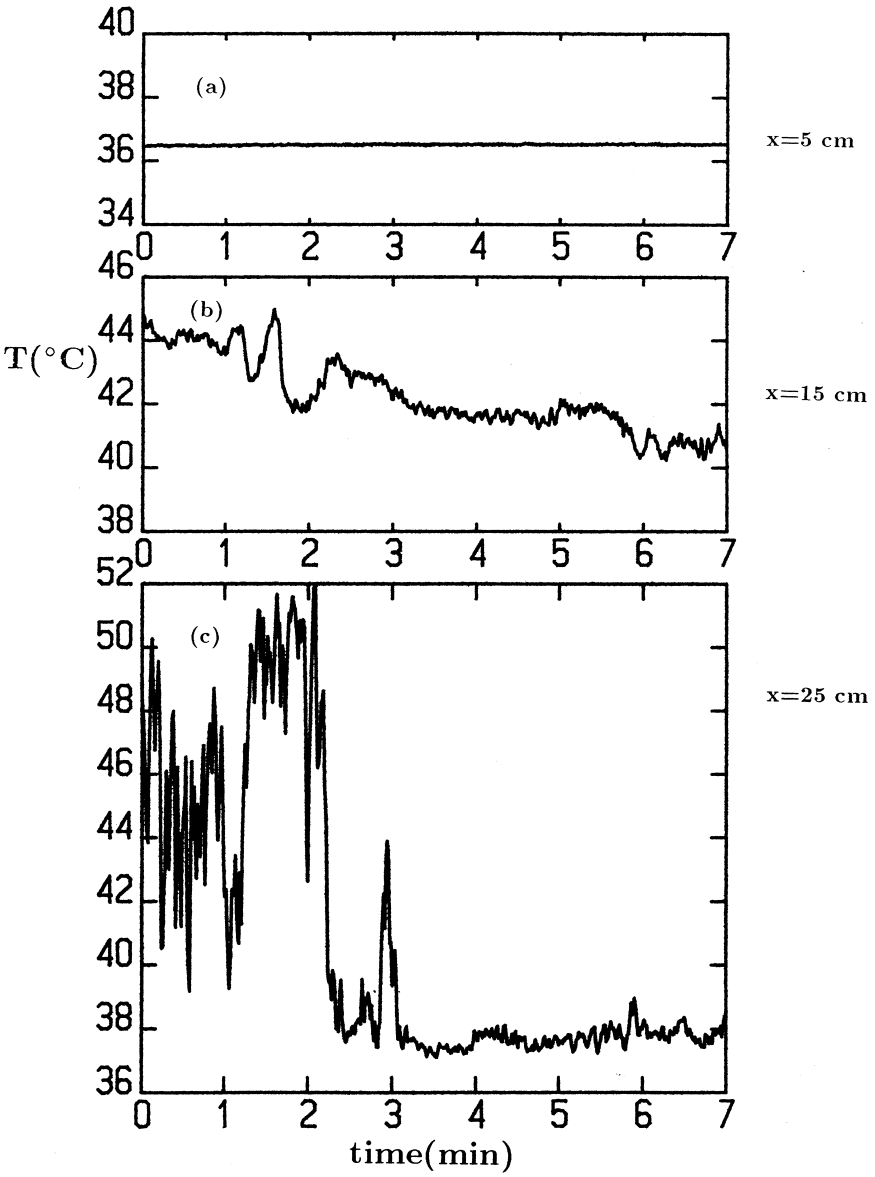

Fig. 7. Temperature fluctuations in a horizontal parallel-plate channel with $Gr/Re^2=60$ and $Re=500$ at (a) $x=5$ cm; (b) $x=15$ cm; (c) $x=25$ cm; (d) $x=31$ cm; (e) $x=36$ cm; (f) $x=44$ cm.

stage, as shown in Fig. 8c, where interaction and combination of vortices have already occurred. However, the amplitude of temperature fluctuation is still very small. This suggests again that the process of interaction and combination between vortices does not cause significant oscillation of flow. The complex flow occurred is still very steady and laminar. When the longitudinal convection rolls are well established in the downstream close to the exit, the temperature fluctuation there, as shown in Fig. 8c, is still not intense. The small fluctuation of temperature suggests that the longitudinal convection roll is still laminar. The decrease in mean temperature for $x=5$ cm to $x=15$ cm suggests that the relatively intense activities of plume and vortex has suck away some of the fluid in the heated layer and make the layer thinner. Therefore, a significant enhancement in heat transfer by the secondary flow can be expected in this region.

For $Gr/Re^2=10$ and $Re=1000$, the mainstream velocity is relatively high while the buoyancy force is still not very low and the bottom heated layer is relatively thick. A very regular periodic oscillation of temperature is found from the region near the entrance to the exit.

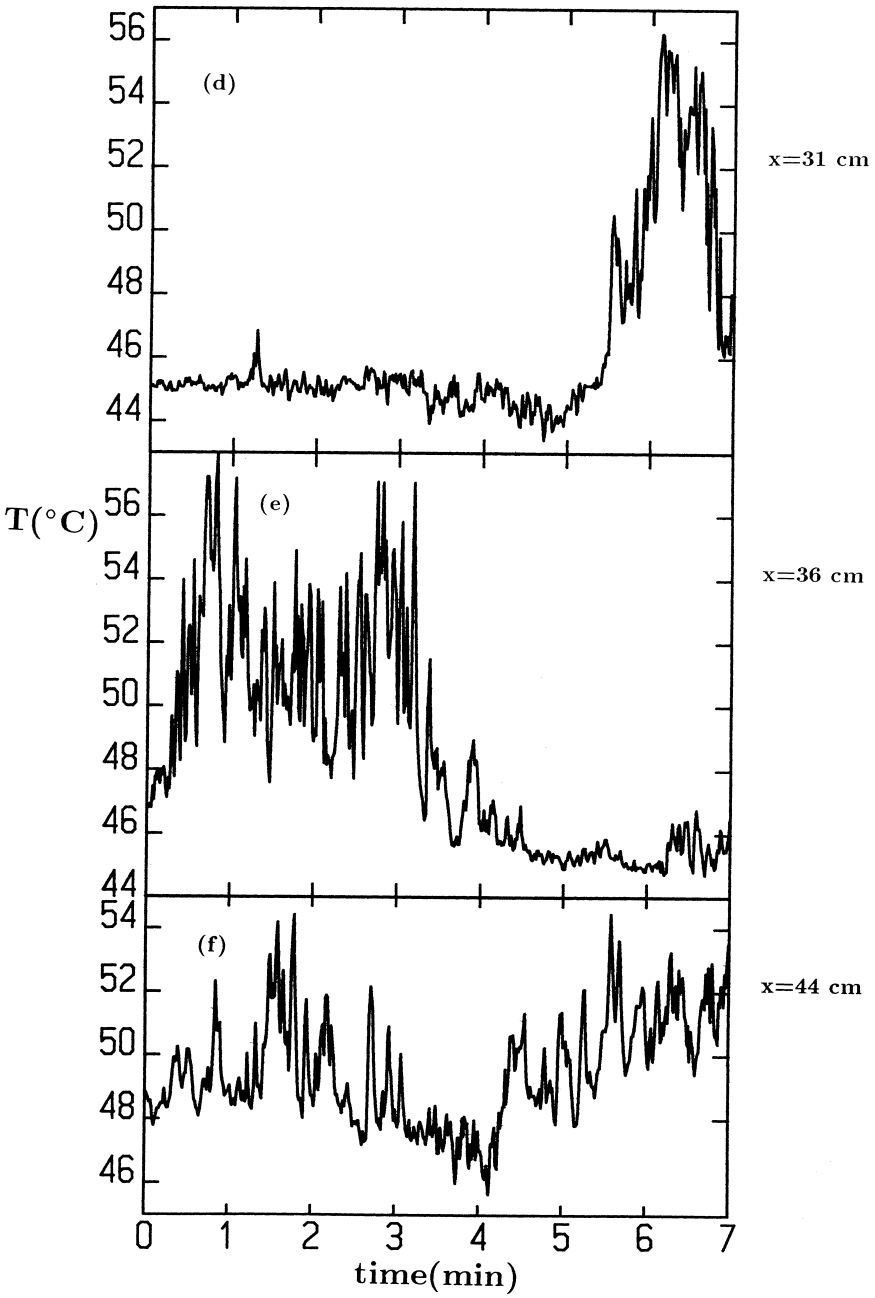

Fig. 7 (*continued*)

Even when the protrusion of plume has not occurred, small oscillation of temperature can also be found, as shown in Fig. 9a and b. All the frequencies of the fluctuations at streamwise locations along the center line are the same, which is seven cycle per minute. One can conclude again that the oscillation of flow is attributed to the relatively high speed flow moving over a thick and unstable heated layer. However, the oscillation of flow measured may be in the spanwise or streamwise direction. The amplitude of fluctuation increases significantly in the downstream region, as shown in Fig. 9c, when protrusion of plume occurs. Oscillation of plume found in the flow visualization experiments is caused by the same mechanism described above, which causes fluctuations of tem-

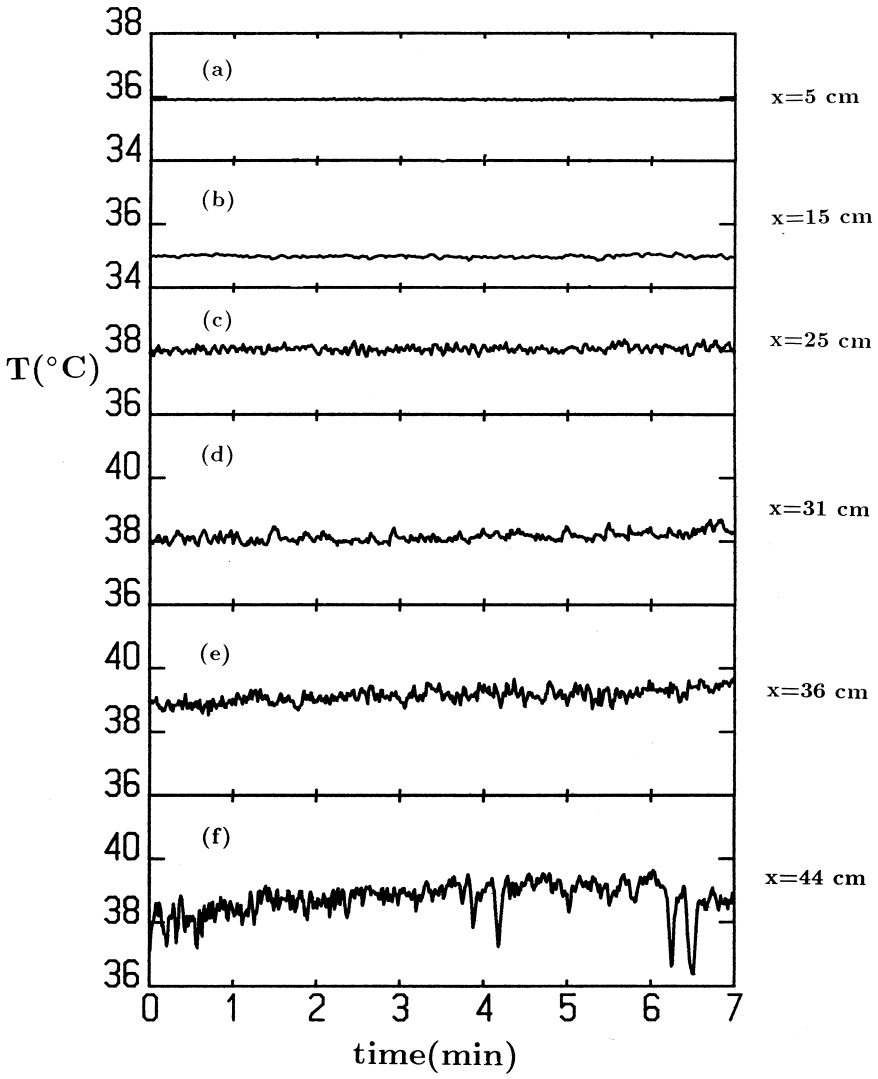

Fig. 8. Temperature fluctuations in a horizontal parallel-plate channel with $Gr/Re^2=450$ and $Re=105$ at (a) $x=5$ cm; (b) $x=15$ cm; (c) $x=25$ cm; (d) $x=31$ cm; (e) $x=36$ cm; (f) $x=44$ cm.

perature. Near the exit, the mushroom-shaped vortex extends laterally far enough to cause interaction with neighboring vortices. This causes additional oscillations of temperature, as shown in Fig. 9f. The gradually increase in the mean temperature toward downstream over most of the channel (except near the exit) suggests that no significant enhancement in heat transfer by the secondary flow is expected.

3.2.2. Convergent channel

For convergent channel, the flow is very stable due to stabilization effect of flow acceleration. No oscillation of temperature was found even for the extreme case when buoyancy parameter is relatively large, as shown in Fig. 10 with $Gr/Re^2=60$ and $Re=500$. The plume and associated vortex activity is still observed. However, the stabilization effect of flow acceleration makes them very stable and no occurrence of any interaction or combinations with the neighboring vortex. This leads to a stable growth of bottom heated layer and a gradual increase in mean temperature, as shown in Fig. 10a–e, except in the exit where large heat loss occurs. Therefore, significant enhancement of heat transfer by the secondary flow is not expected to occur.

The most unstable situation, i.e., $Gr/Re^2=10$ and $Re=1000$, the large amplitude of temperature fluctuations is greatly reduced by the stabilization effect of flow acceleration, as shown in Fig. 11. However, one can

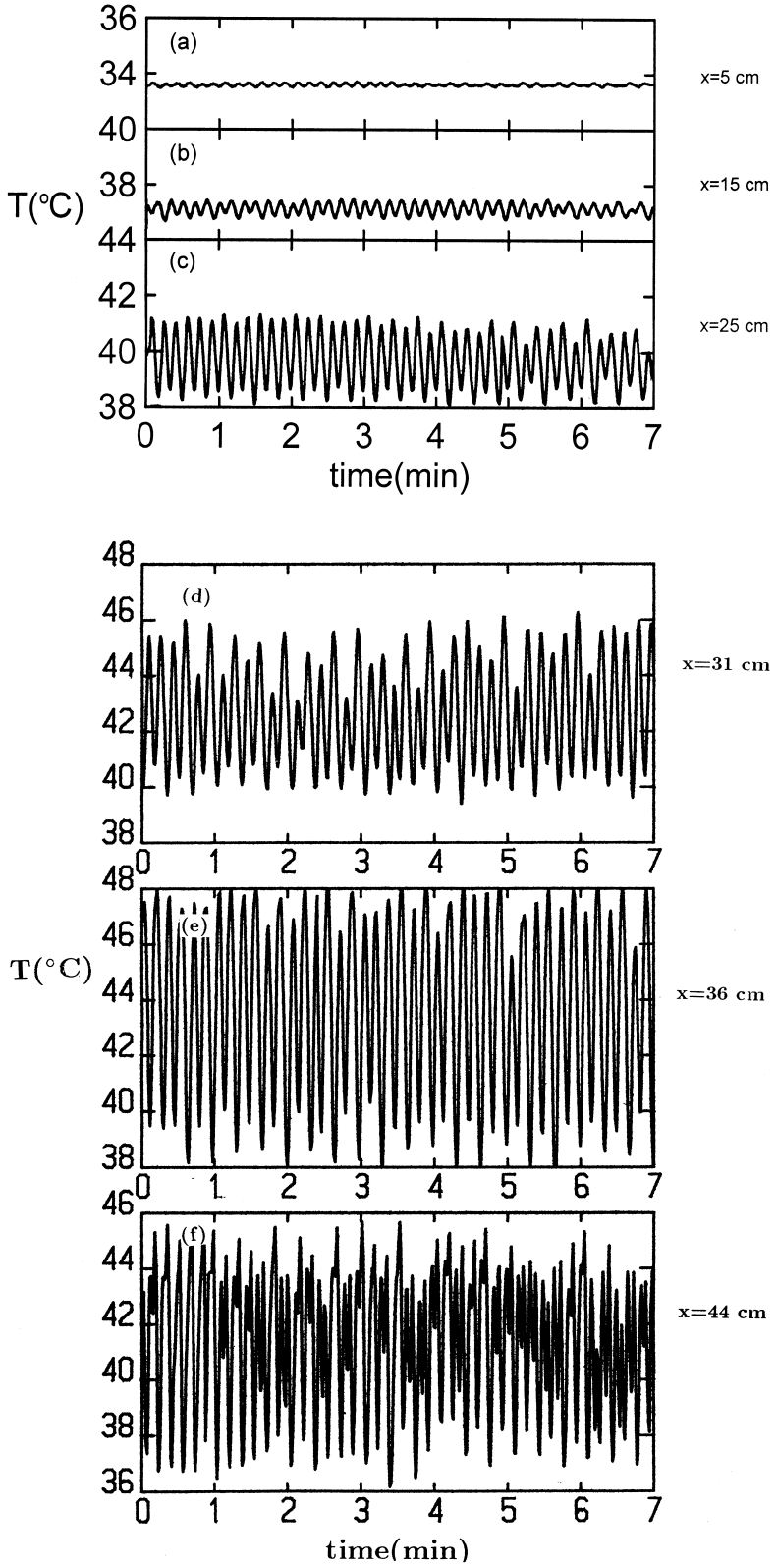

Fig. 9. Temperature fluctuations in a horizontal parallel-plate channel with $Gr/Re^2 = 10$ and $Re = 1000$ at (a) $x = 5$ cm; (b) $x = 15$ cm; (c) $x = 25$ cm; (d) $x = 31$ cm; (e) $x = 36$ cm; (f) $x = 44$ cm.

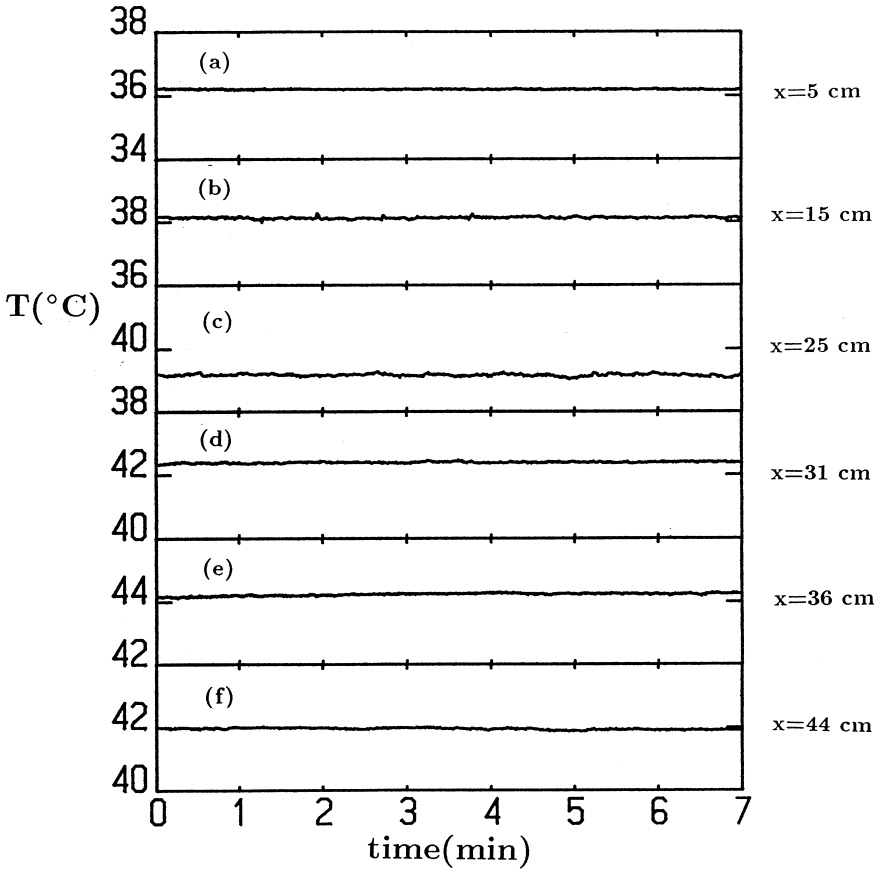

Fig. 10. Temperature fluctuations in a horizontal convergent channel with $Gr/Re^2 = 60$ and $Re = 500$ at (a) $x = 5$ cm to (f) $x = 44$ cm.

still find the growth of amplitude in the upstream region. It appears that in the downstream region the stabilization effect becomes more significant which causes the gradual reduction in amplitude. The frequency of temperature fluctuations is approximately eight cycles per min, which is slightly higher than the case of parallel-plate channel. The slight increase in frequency of temperature fluctuations due to the effect of flow acceleration is not very clear at present stage.

3.3. Mixed convection heat transfer

The current combined entry region Nusselt number results for the parallel-plate channel are compared with the prediction for the pure forced convection and the thermal entry region data of Maughan and Incropera [14], as shown in Fig. 12. As expected, the current Nusselt number results and the prediction for the combined entry condition are significantly higher than the data of Maughan and Incropera [14] and the prediction for the thermal entry condition. For the combined entry condition, the Nusselt number results deviates gradually from the prediction as flow moves downstream and the deviation becomes significant in the downstream due to the occurrence of the rising plume which reduces the thickness of the bottom heated layer and results in the enhancement of heat transfer. It appears that the Nusselt number for the combined entry condition deviates earlier from the pure forced convection results than that for the thermal entry condition, and is more sensitive to the change of the Grashof number. Slight increase in the Grashof number can cause a significant increase in the Nusselt number. The earlier and greater enhancement of the heat transfer for the combined entry condition is attributed to its greater convective heat transfer coefficient that makes the bottom heated layer to grow thicker and become more readily to protrude to the core as a rising plume. That means that the occurrence of the secondary flow for the combined entry condition is earlier than for the thermal entry condition. However, this result could not be confirmed from the comparison of present flow visualization data with others [3, 4] since the present boundary conditions imposed are different from others.

The earlier deviation of the Nusselt number from the

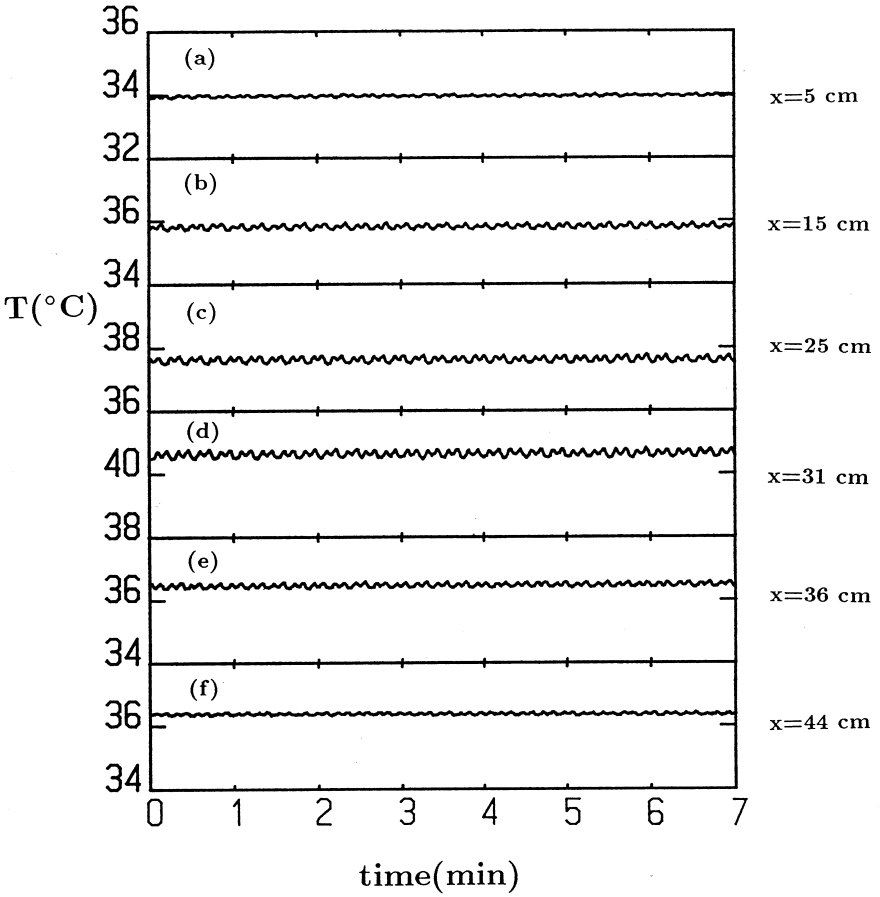

Fig. 11. Temperature fluctuations in a horizontal convergent channel with $Gr/Re^2=10$ and $Re=1000$ at (a) $x=5$ cm; (b) $x=15$ cm; (c) $x=25$ cm; (d) $x=31$ cm; (e) $x=36$ cm; (f) $x=44$ cm.

pure forced convection and greater enhancement in the heat transfer also occur when the Reynolds number is lower, as shown in Fig. 12b. The slight oscillation of the Nusselt number along the axial direction of the channel can be found as those reported in the data of Maughan and Incropera [15] for air flow. However, the oscillation amplitude of the Nusselt number found in the water flow [7] is significantly large. Incropera et al. [7] attributed the first oscillation as the occurrence of the secondary flow and the second oscillation as a transition from laminar to the turbulent flow. However, the previous flow visualization and the temperature fluctuation measurements do not indicate occurrence of turbulence. It is highly probable that one was turbulent and the other not. From further comparison, one can conclude that the first rise of the Nusselt number is due to the protrusion of the plume which gradually suck away the bottom heated layer and make a direct contact of the upper cold fluid with the hot wall. The later decrease of the Nusselt number is attributed to the formation and the later thickening of a new bottom heated layer. However, the second rise of the Nusselt number is not so significant and the current data are not sufficient to make a clear conclusion.

In order to eliminate the Reynolds number effect in the presentation, the Nusselt number is defined based on the air temperature at the inlet of the channel and is normalized by $Re^{0.4}$. For pure forced convection, the normalized Nusselt number $Nu/Re^{0.4}$ is found to be independent of the Reynolds number [34, 35]. For mixed convection in the horizontal channel, the Reynolds number effect on the normalized Nusselt number was found negligible [35]. Therefore, the normalized Nusselt number results at different buoyancy parameter Gr/Re^2 are chosen to present the heat transfer data, as shown in Fig. 13. The increase of buoyancy parameter Gr/Re^2 is achieved by decreasing the Reynolds number. The normalized Nusselt number increases with increasing the buoyancy parameter. The first oscillation of the Nusselt number still exist due to the protrusion and rise up of the bottom heated layer, and the downwash of the upper cold flow. However, the second oscillation of the normalized Nusselt number does not appear. One can clearly find

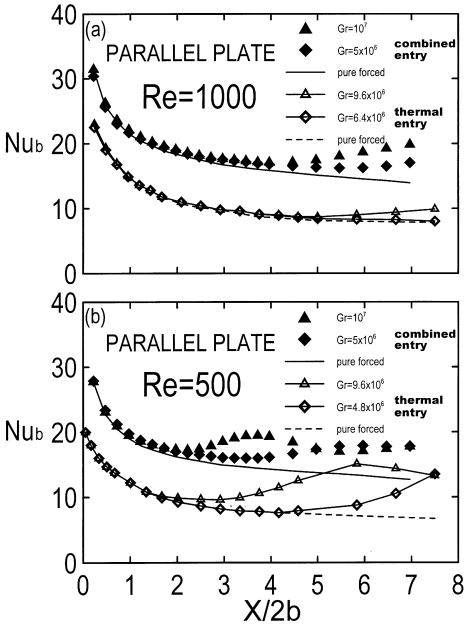

Fig. 12. Comparisons of Nusselt numbers with published results; (a) $Re = 1000$, and (b) $Re = 500$.

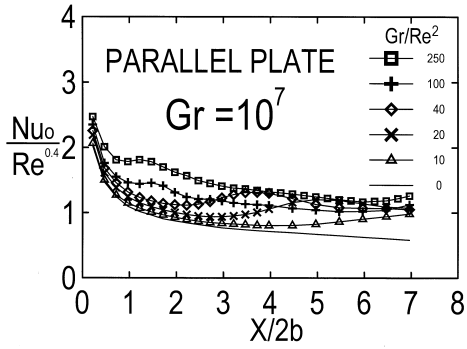

Fig. 13. $Nu/Re^{0.4}$ distributions at different Gr/Re^2 in a horizontal parallel-plate channel.

that the occurrence of the Nusselt number oscillation moves upstream as the buoyancy parameter increases. This is apparently attributed to the fact that the occurrence for the protrusion of the bottom heated layer moves upstream as the buoyancy parameter increases or the Reynolds number decreases, as those found and discussed in the previous section of flow visualization. It appears that in the downstream region the enhancement of heat transfer by the buoyancy parameter is not so large as those shown in Fig. 12. This is due to the use of T_0 as a reference temperature to define both h and Nu. However, the use of T_b as reference temperature can make a larger increase of Nu_b, as shown in Fig. 12.

For convergent channel, the mainstream accelerates

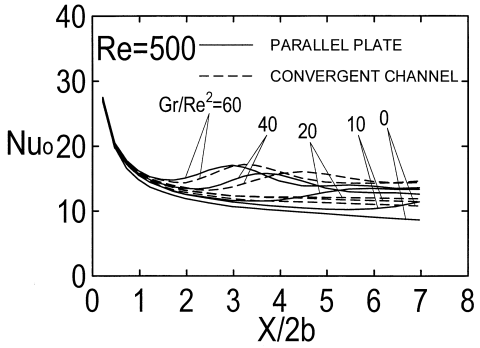

Fig. 14. Comparison of the Nusselt number distributions at different Gr/Re^2 between the case of a horizontal parallel-plate channel and the case of a convergent channel.

that rapid flow velocity occurs in the downstream which can make the heat transfer there higher than the case of the parallel-plate channel. The high speed flow of mainstream in the downstream can make the transport process there dominated by the pure forced convection. In the upstream region where acceleration of flow is not so significant, the buoyancy force still does not play a significant role to enhance the heat transfer. This leads to the results that the normalized Nusselt number at different buoyancy parameters approach a single line, as shown in Fig. 14, when the buoyancy parameter is small and less than 20. When the buoyancy parameter becomes greater ($\geqslant 40$), one can clearly find the enhancement of the heat transfer due to the buoyancy force. However, the later initiation of the secondary flow as indicated previously in both the flow visualization and the temperature fluctuation measurements causes the later enhancement of the heat transfer. In addition, the enhancement of the heat transfer in the convergent channel is not so significant as in the case of the parallel plate channel. This is apparently due to the stabilizing effect of the accelerated flow in the convergent channel.

4. Conclusions

Secondary flow structure and enhancement of heat transfer in a bottom heated horizontal parallel-plate or convergent channel has been investigated experimentally. Secondary flow appearing as mushroom-shaped plume associated with vortices is found. The number of plumes produced is much less and the size of the plume is much greater than those formed in the experiments with water. Instead of the Grashof number, the number of plumes produced is proportional to the Rayleigh number. Due to the lateral extension and combination of the vortices, two-dimensional longitudinal convection rolls can be formed in the downstream region. The combination between the neighboring vortices causes the number of

the convection rolls produced in the experiments with air much less than the number of vortex rolls formed in the experiments with water. For the convergent channel, the acceleration of the mainstream can make the bottom heated layer thinner which delays the initiation of the secondary flow, and stabilize the flow and suppress the interactions between neighboring plumes. The plumes occurred are very steady and laminar in the entire channel, resulting in a smaller and later enhancement of heat transfer than the case of the parallel-plate channel.

Temperature fluctuation measurements at different locations are used to infer the detailed flow structure and the initiation and oscillation of the bottom heated layer and the secondary flow. The flow structure inferred confirms with the flow visualization results. The convergence of the channel can suppress the temperature fluctuations due to the stabilization effect of the favorable pressure gradient.

The Nusselt numbers divided by $Re^{0.4}$ are found to be a suitable way to present the data. The Nusselt number increases with increasing Gr/Re^2. In addition, the locations for both the onset of heat transfer enhancement and the maximum Nusselt number move upstream as Gr/Re^2 increases. The heat transfer enhancement in the convergent channel occurs in a later stage and is less pronounced than in the parallel-plate channel due to the stabilization effect of the accelerated flow.

Acknowledgement

This research was sponsored by the National Science Council of Taiwan under contract No. NSC 87-2212-E006-088.

References

[1] R.R. Gilpin, H. Imura, K.C. Cheng, Experiments on the onset of longitudinal vortices in horizontal Blasius flow heated from below, ASME J. Heat Transfer 100 (1978) 71–77.

[2] J.R. Maughan, F.P. Incropera, Experiments on mixed convection heat transfer for airflow in a horizontal rectangular and inclined channel, Int. J. Heat Mass Transfer 30 (1987) 1307–1318.

[3] G.J. Hwang, C.L. Liu, An experimental study of convective instability in the thermal entrance region of a horizontal parallel-plate channel heated from below, Can. J. Chem. Engng 54 (1976) 521–525.

[4] Y. Kamotani, S. Ostrach, H. Miao, Convective heat transfer augmentation by means of thermal instability, ASME J. Heat Transfer 101 (1979) 222–226.

[5] Y. Mori, Y. Uchida, Forced convection heat transfer between horizontal flat plate, Int. J. Heat Mass Transfer 9 (1966) 803–817.

[6] D.G. Osborne, F.P. Incropera, Laminar, mixed convection heat transfer for flow between horizontal parallel plates with asymmetric heating, Int. J. Heat Mass Transfer 28 (1985) 207–217.

[7] F.P. Incropera, A.L. Knox, J.R. Maughan, Mixed convection flow and heat transfer in the entry region of a horizontal rectangular duct, ASME J. Heat Transfer 109 (1987) 434–439.

[8] E.J. Davis, C.K. Choi, Cellular convection with liquid-film flow, J. Fluid Mech. 81 (3) (1977) 565–592.

[9] Y. Kamotani, S. Ostrach, Effect of thermal instability on thermally developing laminar channel flow, ASME J. Heat Transfer 98 (1976) 62–66.

[10] M. Akiyama, G.H. Hwang, K.C. Cheng, Experiments in the onset of longitudinal vortices in laminar forced convection between horizontal plates, ASME J. Heat Transfer 93 (1971) 335–341.

[11] S. Ostrach, Y. Kamotani, Heat transfer augmentation in laminar fully developed channel flow by means of heating from below, ASME J. Heat Transfer 97 (1975) 220–225.

[12] K.C. Chiu, J. Ouazzani, F. Rosenberger, Mixed convection between horizontal plates—II. Fully developed flow, Int. J. Heat Mass Transfer 30 (1987) 1655–1662.

[13] K.C. Chiu, J. Ouazzani, F. Rosenberger, Mixed convection between horizontal plates—I. Entrance effects, Int. J. Heat Mass Transfer 30 (1987) 1645–1654.

[14] J.R. Maughan, F.P. Incropera, Regions of heat transfer enhancement for laminar mixed convection in a parallel plate channel, Int. J. Heat Mass Transfer 33 (1990) 555–570.

[15] F.S. Lee, G.J. Hwang, Transient analysis on the onset of thermal instability in the thermal entrance region of a horizontal parallel-plate channel, ASME J. Heat Transfer 113 (1991) 363–370.

[16] F.S. Lee, G.J. Hwang, The effect of asymmetric heating on the onset of thermal instability in the thermal entrance region of a parallel-plate channel, Int. J. Heat Mass Transfer 34 (1991) 2207–2218.

[17] J.N. Lin, F.C. Chou, P.Y. Tzeng, Theoretical prediction of the onset of thermal instability in the thermal entrance region of horizontal rectangular channels, Int. J. Heat Fluid Flow 12 (1991) 218–224.

[18] M.M.M. Abou-Ellail, S.M. Morcos, Buoyancy effects in the entrance region of horizontal rectangular channels, ASME J. Heat Transfer 105 (1983) 152–159.

[19] H.V. Mahaney, F.P. Incropera, S. Ramadhyani, Development of laminar mixed convection in the thermal entrance region of horizontal rectangular ducts, Num. Heat Transfer 12 (1987) 137–155.

[20] J.R. Maughan, F.P. Incropera, Fully developed mixed convection in a horizontal channel heated uniformly from above and below, Num. Heat Transfer, A 17 (1990) 417–430.

[21] F.C. Chou, G.J. Hwang, Vorticity-method for Graetz problem with the effect of natural convection in a horizontal rectangular channel with uniform wall heat flux, ASME J. Heat Transfer 109 (1987) 704–710.

[22] J.N. Lin, F.C. Chou, Laminar mixed convection in the thermal entrance region of horizontal isothermal rectangular channels, Can. J. Chem. Engng 67 (1989) 361–367.

[23] T.A. Nyce, J. Ouazzani, Durand-Daubin, A, F. Rosen-

berger, Mixed convection in a horizontal rectangular channel—experimental and numerical velocity distributions, Int. J. Heat Mass Transfer 35 (1992) 1481–1494.
[24] B.L. Reeves, C.J. Kippenhan, On a particular class on similar solutions of the equations of motion and energy of a viscous fluid, J. Aerospace Sci. 29 (1962) 38–47.
[25] E.M. Sparrow, J.B. Starr, Heat transfer to laminar flow in tapered passages, ASME J. Appl. Mech. 32 (1965) 684–689.
[26] Y. Shiina, Heat transfer in a tapered passage, Int. J. Heat Fluid Flow 8 (1987) 64–71.
[27] J.W. Yang, G.W. Price, Laminar flow development and heat transfer in convergent plane-walled channels, Appl. Sci. Res. 25 (1972) 361–371.
[28] J.W. Yang, N. Liao, An experimental study of turbulent heat transfer in converging rectangular ducts, ASME J. Heat Transfer 95 (1973) 453–547.
[29] C.C. Su, H. Lin, Forced convection in convergent and divergent ducts of rectangular cross section, Num. Heat Transfer, Part A 20 (1991) 445–458.
[30] C.C. Su, H. Lin, Forced convection in the entrance region of convergent and divergent ducts of rectangular cross section, J. CSME 12 (3) (1991) 314–319.
[31] H. Tanaka, H. Kawamura, A. Tateno, S. Hatamiya, Effect of laminarization and retransition on heat transfer for low Reynolds number flow through a converging to constant area duct, ASME J. Heat Transfer 104 (1982) 363–371.
[32] K.R. Mutama, H. Iacovides, The investigation of developing flow and heat transfer in a long convergent duct, ASME J. Heat Transfer 115 (1993) 897–903.
[33] C. Gau, T.M. Huang, C.W. Liu, W. Aung, Mixed convection flow and heat transfer in a horizontal divergent channel with bottom wall heated, Proceedings of the 11th International Heat Transfer Conference, vol. 3, 1998, pp. 257–262.
[34] T.M. Huang, C. Gau, W. Aung, Mixed convection flow and heat transfer in a vertical convergent channel, Int. J. Heat Mass Transfer 38 (13) (1995) 2445–2456.
[35] T.M. Huang (1994) Mixed convection flow and heat transfer in a heated convergent or divergent channel. Ph.D Thesis, National Cheng Kung University, Tainan, Taiwan
[36] B.W. Webb, D.P. Hill, High Rayleigh number laminar natural convection in an asymmetrically heated vertical channel, ASME J. Heat Transfer 111 (1989) 649–656.
[37] R.A. Wirtz, P. McKinley, Buoyancy effects on downward laminar convection between parallel-plates, in: Fundamentals of Forced and Mixed Convection, ASME HTD (42), 1985, pp. 105–112.
[38] S.J. Kline, F.A. McClintock, Describing uncertainties in single-sample experiments, Mech. Engng 75 (1953) 3–12.